RESEARCH ARTICLE

NANO · MICRO small
www.small-journal.com

Heterostructured Graphene@Silica@Iron Phenylphosphinate for Fire-Retardant, Strong, Thermally Conductive Yet Electrically Insulated Epoxy Nanocomposites

Qiang Chen, Siqi Huo, Yixia Lu, Mingmei Ding, Jiabing Feng, Guobo Huang, Hang Xu, Ziqi Sun, Zhengzhou Wang,* and Pingan Song**

The portfolio of extraordinary fire retardancy, mechanical properties, dielectric/electric insulating performances, and thermal conductivity (λ) is essential for the practical applications of epoxy resin (EP) in high-end industries. To date, it remains a great challenge to achieve such a performanceportfolio in EP due to their different and even mutually exclusive governing mechanisms. Herein, a multifunctional additive (G@SiO_2@FeHP) is fabricated by in situ immobilization of silica (SiO_2) and iron phenylphosphinate (FeHP) onto the graphene (G) surface. Benefiting from the synergistic effect of G, SiO_2 and FeHP, the addition of 1.0 wt% G@SiO_2@FeHP enables EP to achieve a vertical burning (UL-94) V-0 rating and a limiting oxygen index (LOI) of 30.5%. Besides, both heat release and smoke generation of as-prepared EP nanocomposite are significantly suppressed due to the condensed-phase function of G@SiO_2@FeHP. Adding 1.0 wt% G@SiO_2@FeHP also brings about 44.5%, 61.1%, and 42.3% enhancements in the tensile strength, tensile modulus, and impact strength of EP nanocomposite. Moreover, the EP nanocomposite exhibits well-preserved dielectric and electric insulating properties and significantly enhanced λ. This work provides an integrated strategy for the development of multifunctional EP materials, thus facilitating their high-performance applications.

1. Introduction

Epoxy resin (EP), as one of the most important thermosetting resins, has been ubiquitously utilized in various fields, such as adhesives, coatings, household appliances, communication equipment, and electric/electronic packages, owing to its high adhesion, great electrical insulation, and good mechanical properties and chemical resistance.[1–3] However, the inherent flammability and poor smoke suppression of EP significantly restrict its real-world applications.[4–6] For this reason, the advanced EP materials with satisfactory fire-retardant performances are highly desired in recent years.

Over the past few decades, incorporating eco-friendly phosphorus/nitrogen (P/N)-containing flame retardant into EP is the most common approach to confer fire safety.[7–9] Although these flame retardants show good fire-retardant efficiency

Q. Chen, M. Ding, H. Xu
Key Laboratory of Integrated Regulation and Resource Development on Shallow Lakes
Ministry of Education
College of Environment
Hohai University
No.1 Xikang Road, Nanjing 210098, China
E-mail: xuhang810826@hhu.edu.cn

S. Huo, Y. Lu, P. Song
Centre for Future Materials
University of Southern Queensland
Springfield 4300, Australia
E-mail: pingan.song@usq.edu.au

J. Feng
China-Australia Institute for Advanced Materials and Manufacturing
Jiaxing University
Jiaxing 314001, China

The ORCID identification number(s) for the author(s) of this article can be found under https://doi.org/10.1002/smll.202310724

DOI: 10.1002/smll.202310724

G. Huang
School of Pharmaceutical and Materials Engineering
Taizhou University
1139 Shifu Road, Taizhou 318000, China

Z. Sun
School of Mechanical
Medical and Process Engineering
School of Chemistry and Physics
Queensland University of Technology
2 George Street, Brisbane, QLD 4001, Australia

Z. Wang
School of Materials Science and Engineering
Tongji University
Shanghai 201804, China
E-mail: zwang@tongji.edu.cn

Z. Wang
Key Laboratory of Advanced Civil Engineering Materials (Tongji University)
Ministry of Education
Shanghai 201804, China

P. Song
School of Agriculture and Environmental Science
University of Southern Queensland
Springfield 4300, Australia

towards EP, they usually suffer from the adverse effects on the mechanical properties because of their plasticizing effect.[10,11] For instance, He et al. reported that incorporating 10 wt% imide-9,10-dihydro-9-oxa-10-phosphaphenanthrene-10-oxide derivative (BMP) into EP increased the UL-94 rating to V-0 and led to 30.3% and 26.4% reductions in the peak heat release rate (PHRR) and total smoke production (TSP), but reducing the tensile strength by 7.8%.[12] Yang et al. prepared a flame-retardant EP thermoset by adding 6.0 wt% of (2-phenyl-1,3,2-dioxaborolan-4-yl) methanamine ammonium polyphosphate (PBMA-APP), of which the UL-94 classification increased to V-0 and total heat release (THR) and TSP reduced by 29.8% and 32.3%, respectively.[13] However, the tensile strength of the obtained EP thermoset was decreased by 13.2% relative to that of pure EP. Therefore, it is still highly challenging to develop multifunctional flame retardants for the fabrication of fire-safe and mechanically-robust EP materials. In addition, the P/N-containing flame retardants usually exhibit poor thermal conductivity (λ), significantly restricting their applications in high-performance EP materials.[6]

To overcome these dilemmas, a great deal of researches have been conducted to improve the fire-retardant, mechanical and thermally conductive properties of EP by incorporating P/N-functionalized nanofillers.[14–17] Among various nanofillers, graphene (G), as a 2D layered nanomaterial, has gained great attention owing to its high specific surface area, outstanding mechanical properties, excellent thermally conductivity, and good chemical resistance.[18,19] The surface functionalization by using P/N-based organics can endow G with good compatibility with EP matrix, which leads to the satisfactory mechanical and thermally conductive performances of EP composites.[20] Meanwhile, G can serve as a physical barrier to inhibit the release of heat and smoke during combustion of the EP matrix.[21] For example, Wang et al. synthesized a polyphosphamide-functionalized G nanomaterial, and 8.0 wt% of it reduced the PHRR and TSP of EP composite by 41.3% and 12.7% and increased the tensile strength by 19.4%.[22] Despite such an encouraging advancement, the fire retardancy and mechanical properties of the G-containing EP materials are far from satisfactory. Meanwhile, the G-based flame retardants usually tend to deteriorate the electric/dielectric properties of EP. Therefore, it is critical to further enhance the flame-retardant and mechanically-reinforcing effects of G-based flame retardants and eliminate their detrimental effect on the electric/dielectric properties.

Metal-organic phosphonate usually shows good compatibility with the EP matrix due to its tailorable structure consisting of central metal ions and organic P/N-derived linkers. Besides, it can greatly enhance the fire retardancy and smoke suppression of EP.[23–25] To date, different types of metal-organic phosphonate functionalized G hybrids have been constructed for the fabrication of fire-safe EP composites.[26,27] For instance, Wang et al. reported that with 3.0 wt% of zinc *N, N'*-piperazine (bismethylene phosphonate) grafted reduced graphene oxide (rGO@ZnPB), the EP composite exhibited 27.0% and 25.1% decreases in PHRR and total smoke release (TSR) relative to those of the untreated EP.[28] Zhu et al. synthesized iron hexamethylenediaminetetrakis-(methylenephosphonate) modified reduced graphene oxide (Fe-rGO) for EP.[29] When 2.0 wt% of Fe-rGO was added, the EP composite achieved 40.0% and 43.3% reductions in PHRR and THR in comparison to pure EP. However, these metal-organic phosphonate modified G nanomaterials suffer from low flame-retardant efficiencies, and usually need high additions to impart a UL-94 V-0 rating.

Recently, to raise the fire-retardant efficiency of P/N-based flame retardants, some other fire-retardant elements (i.e., silicon, sulfur, and boron) are introduced into their structures.[30–32] Silica (SiO_2) has been widely recognized as an environment-friendly synergist for P/N-containing flame retardants due to its excellent thermal stability, inert and non-toxic characteristics.[33,34] For instance, Wang et al. prepared tin ethylenediamine tetramethylene phosphonate (TETP) modified SiO_2 (SiO_2@TETP) for improving the fire safety of EP. At the same dosage of 3.0 wt%, the PHRR, THR, and TSR of EP/SiO_2@TETP composite were reduced by 8.3%, 12.2%, and 15.9% relative to those of EP/TETP, respectively.[35] Thus, it is speculated that combining SiO_2 and metal-organic phosphonate modified G could be helpful for greatly improving the fire-safe, mechanical and thermally conductive properties of EP.

Herein, we report a surface immobilization strategy to fabricate multifunctional G@SiO_2@FeHP by in situ loading SiO_2 nanoparticles and iron phenylphosphinate (FeHP) onto the G surface. The impacts of G@SiO_2@FeHP on the fire retardancy, mechanical properties, dielectric/electric performances and λ of EP were systematically investigated. In addition, the fire-retardant mode-of-action of G@SiO_2@FeHP was explored in detail. Our results clearly demonstrate that the as-designed G@SiO_2@FeHP is a multifunctional, high-efficiency additive, and 1.0 wt% of it can simultaneously improve the fire retardancy, mechanical properties and λ of EP and effectively maintain the electrical insulation and dielectric properties. Thus, G@SiO_2@FeHP is expected to be widely applied in the fabrication of high-performance EP nanocomposites.

2. Results and Discussion

2.1. Synthesis and Characterization of G@SiO_2@FeHP

The synthetic route of G@SiO_2@FeHP is illustrated in **Figure 1a**, which involves the in situ self-assembly of SiO_2 nanoparticles on the G surface and the in situ growth of FeHP on the G@SiO_2 surface. Transmission electronic microscopy (TEM) and scanning electron microscope (SEM) were applied to characterize the surface micro-morphologies of G, SiO_2, G@SiO_2, FeHP and G@SiO_2@FeHP. The G presents a typically flat yet wrinkled sheet-like structure, and it is almost transparent (Figure 1b). As depicted in Figure 1c, the amorphous SiO_2 is irregularly arranged and tends to somewhat aggregate. On the contrary, the SiO_2 nanoparticles with reduced sizes are uniformly located on the G surface (Figure 1d), since the large-aspect-ratio G nanosheets can prevent SiO_2 from aggregating. The formation of G@SiO_2 is mainly due to the facilitation of sodium carboxy methyl cellulose (NaCMC) towards the nucleation and growth of SiO_2 on the G surface.[36]

The TEM image of FeHP illustrates its cuboid-like structure (Figure 1e). After the in situ immobilization, the FeHP layer is uniformly coated on the surface of G@SiO_2 (Figure 1f). The electrostatic interaction between the positively charged FeHP and negatively charged G@SiO_2 results in the formation of positively

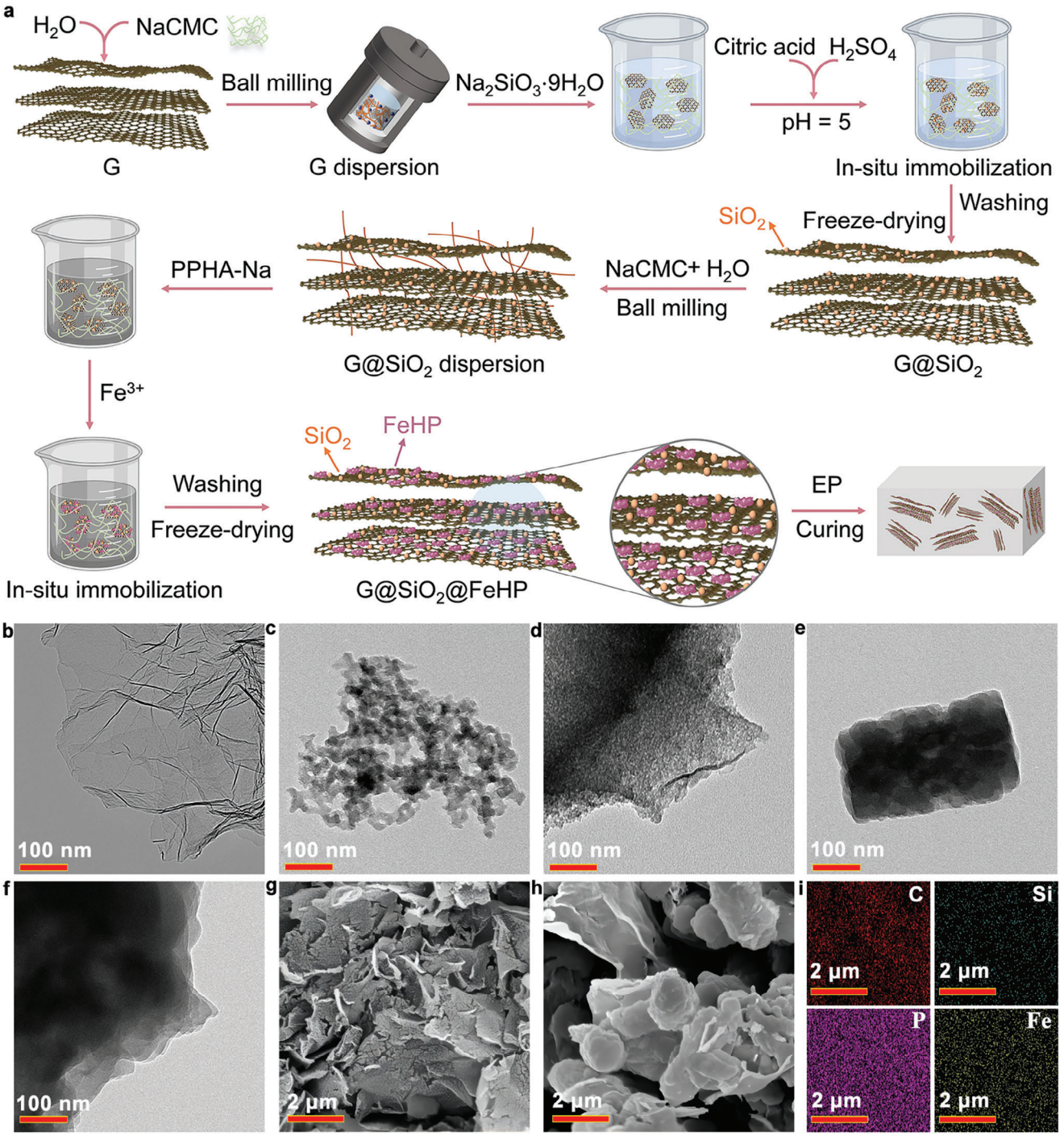

Figure 1. Design and synthesis of $G@SiO_2@FeHP$. a) Synthetic route of $G@SiO_2@FeHP$; TEM images of b) G, c) SiO_2, d) $G@SiO_2$, e) FeHP, and f) $G@SiO_2@FeHP$; SEM images of g) $G@SiO_2$ and h) $G@SiO_2@FeHP$; and i) EDS mapping images of $G@SiO_2@FeHP$.

charged $G@SiO_2@FeHP$.[37] The SEM images show that the surface of $G@SiO_2$ is much rougher than that of G, and the SiO_2 nanoparticles are homogeneously dispersed on the G surface (Figure 1g and Figure S2a,c, Supporting Information). As presented in Figure 1h and Figure S2e (Supporting Information), FeHP uniformly grows onto the surface of $G@SiO_2$. Additionally, the energy dispersive X-ray spectroscopy (EDS) mappings of $G@SiO_2@FeHP$ reveal the even distribution of Si, P, and Fe elements on the G surface. These results manifest the successful in situ immobilization of SiO_2 and FeHP on the G surface, respectively.

The chemical structures of G, SiO_2, FeHP, and $G@SiO_2@FeHP$ were characterized by Fourier transform infrared (FTIR) spectroscopy (**Figure 2**a). For G, the characteristic

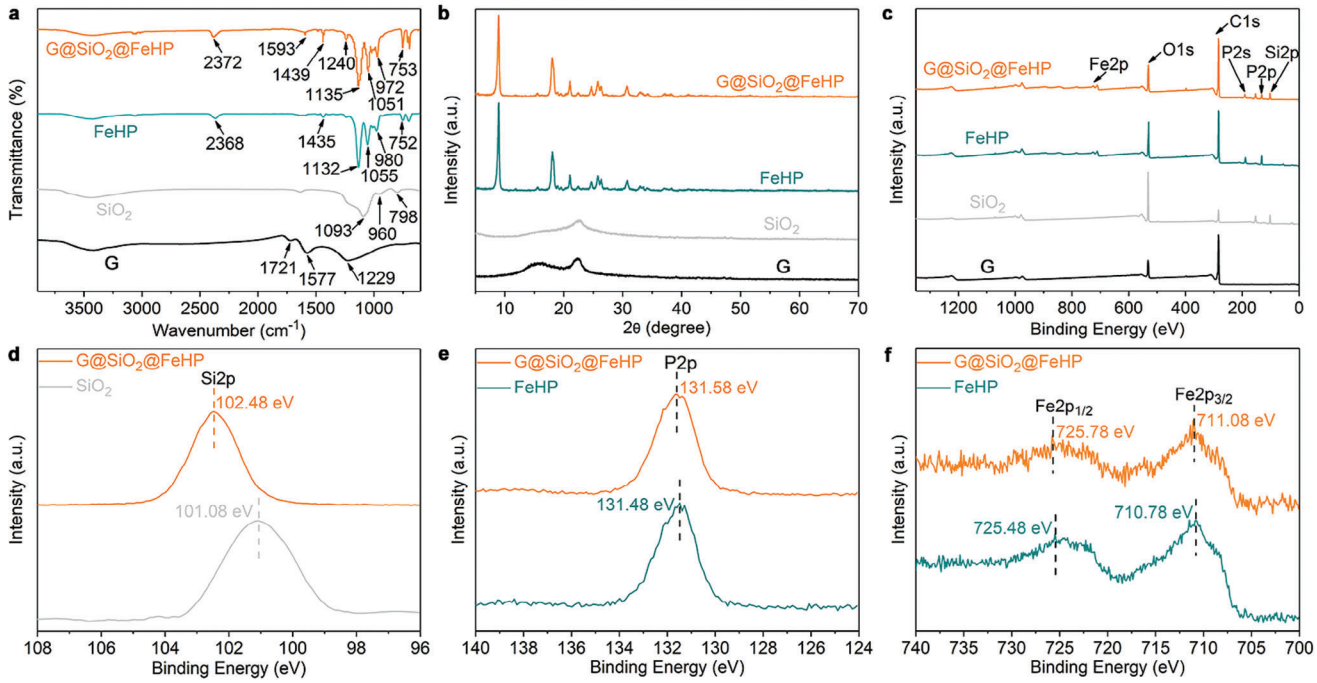

Figure 2. Structural characterizations. a) FTIR spectra, b) XRD patterns, and c) XPS survey spectra of G, SiO_2, FeHP and G@SiO_2@FeHP; d) high resolution Si2p XPS spectra of SiO_2 and G@SiO_2@FeHP; and high resolution e) P2p and f) Fe2p spectra of FeHP and G@SiO_2@FeHP.

peaks at 1229, 1577 and 1721 cm^{-1} belong to the stretching vibrations of C—O—C, C=C and C=O, respectively.[38] The FTIR spectrum of SiO_2 exhibits several absorption peaks around 798, 960 and 1093 cm^{-1}, which are assigned to the bending vibration of Si—O—Si, the stretching vibration of Si—OH and the asymmetric stretching of Si—O—Si, respectively.[39] For FeHP, the band at 2368 cm^{-1} is attributed to the P—H stretching vibration. The peak at 1435 cm^{-1} arises from the C=C stretching vibration of benzene ring, and that at 1132 cm^{-1} is ascribed to the P=O stretching vibration. The absorption peaks of P—O appear at 1055 and 980 cm^{-1}, and that of P—C can be detected at 752 cm^{-1}.[40,41] Notably, G@SiO_2@FeHP shows the characteristic absorption peaks of G, SiO_2 and FeHP in its FTIR spectrum, indicative of the successful in situ immobilization of SiO_2 and FeHP onto the G surface.

The XRD patterns of G, SiO_2, FeHP and G@SiO_2@FeHP are presented in Figure 2b. The diffractogram of G exhibits a broad peak at $2\theta = 22.7°$, corresponding to (002) diffraction. There is also a broad diffraction peak at $2\theta = 22.7°$ in the XRD pattern of SiO_2, indicating its amorphous characteristic.[42] FeHP presents a series of diffraction signals, proving its crystalline structure. Regarding G@SiO_2@FeHP, all diffraction signals of FeHP can be detected at the same 2θ, suggesting that the crystal structure of FeHP is maintained even after growing onto the G@SiO_2 surface. Besides, the diffraction peaks of G and SiO_2 are unobvious in the XRD pattern of G@SiO_2@FeHP, which is probably because the immobilization of FeHP impedes the interaction of the X-rays with G and SiO_2.

X-ray photoelectron spectroscopy (XPS) was conducted to investigate the chemical composition and state of G, SiO_2, FeHP and G@SiO_2@FeHP surfaces, as shown in Figure 2c–f. For G, there are only C1s and O1s peaks. The Si, O, and C elements can be detected on the SiO_2 surface, and the Si2p peak appears at 101.08 eV.[43] For FeHP, the P2p peak can be observed at 131.48 eV, and the $Fe2p_{1/2}$ and $Fe2p_{3/2}$ peaks appear at 725.48 and 710.78 eV, respectively.[44,45] The Fe, P, Si, C, and O elements can be detected on the G@SiO_2@FeHP surface, further indicating the successful immobilization of SiO_2 and FeHP. The binding energy of the Si2p (102.48 eV), P2p (131.58 eV), $Fe2p_{1/2}$ (755.78 eV), and $Fe2p_{3/2}$ (711.08 eV) peaks in G@SiO_2@FeHP is higher than that in SiO_2 or FeHP, suggesting the strong interaction between G, SiO_2, and FeHP.[46,47]

The limiting oxygen index (LOI), vertical burning (UL-94) and cone calorimetry tests were utilized to evaluate the fire retardancy of EP and EP nanocomposites. As shown in **Figure** 3a,b, the neat EP presents a LOI value of 23.5%, and cannot self-extinguish during UL-94 test (no rating), suggesting its highly flammable characteristic. After the addition of G@SiO_2@FeHP, the fire-retardant performances of EP/G@SiO_2@FeHP nanocomposites are significantly improved. In Figure 3a–c and Figure S4 (Supporting Information), the addition of 0.5 wt% G@SiO_2@FeHP enhances the LOI value of EP to 28.5%, and enables it to pass a UL-94 V-1 rating. When 1.0 wt% G@SiO_2@FeHP is incorporated, the LOI value of EP/1.0G@SiO_2@FeHP nanocomposite enhances to 30.5%, and it can self-extinguish within 3.5 s in UL-94 test, thus achieving a V-0 rating. At the same loading level of 1.0 wt%, G@SiO_2@FeHP endows EP with a higher LOI value than G@SiO_2 (25.0%), G@FeHP (30.0%), and simple blending of G, SiO_2 and FeHP (30.0%). The above results indicate that the combination of G, SiO_2 and FeHP by in situ immobilization can obviously improve the fire-retardant performances of EP.

The cone calorimetry test was conducted to assess the combustion behaviors of EP materials. The PHRR and THR of untreated EP are 2074 kW m^{-2} and 173 MJ m^{-2},

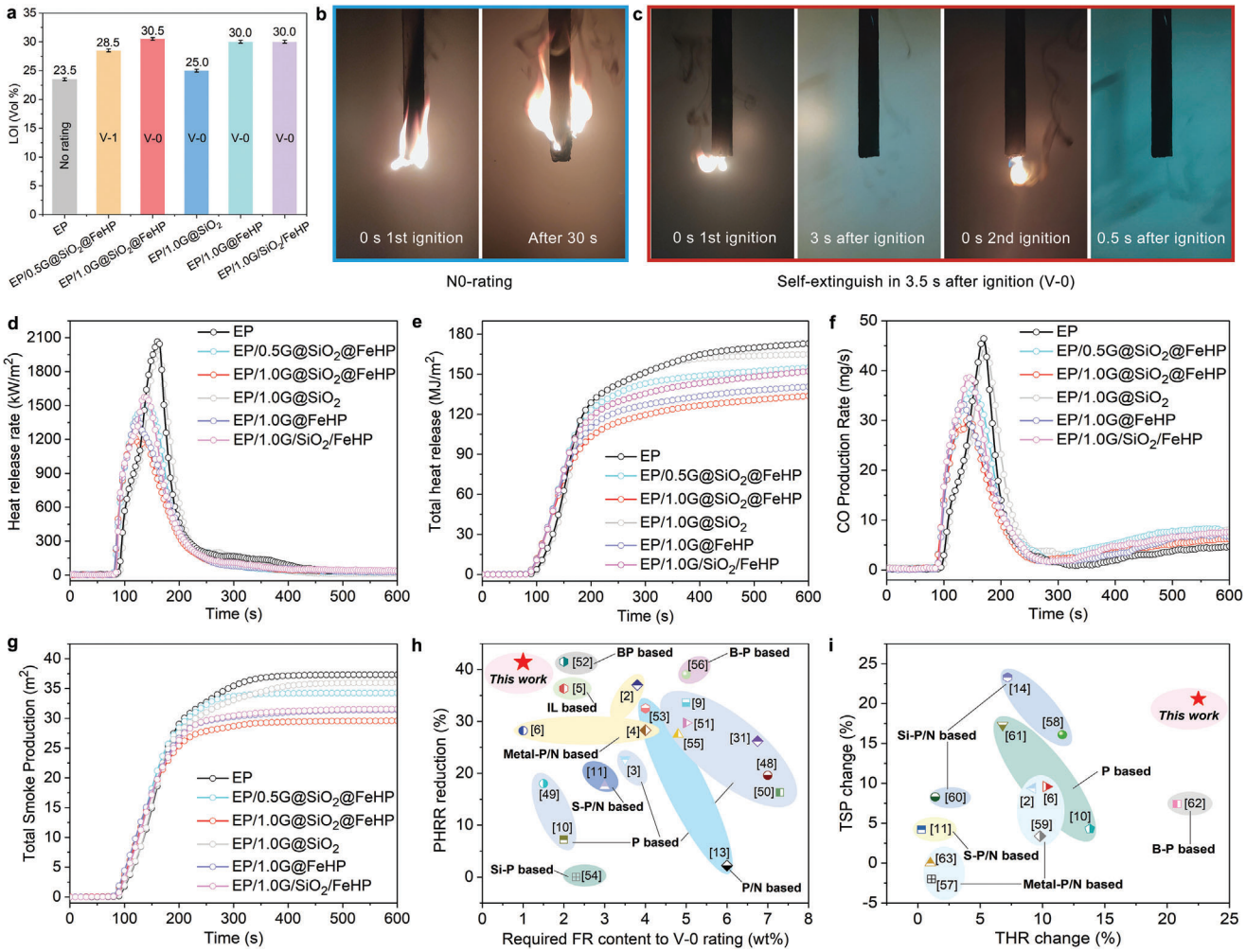

Figure 3. Flame retardancy. a) LOI values of EP and its nanocomposites; digital photographs of b) EP and c) EP/1.0G@SiO_2@FeHP during UL-94 tests; d) heat release rate, e) total release rate, f) CO production rate, and g) TSP curves of EP and its nanocomposites; h) PHRR reductions of EP/1.0G@SiO_2@FeHP nanocomposite and previous fire-retardant EP materials as a function of required fire-retardant content to reach a UL-94 V-0 rating; and i) THR and TSP variations of EP/1.0G@SiO_2@FeHP nanocomposite and previously reported fire-retardant EP materials (filler addition: 1.0 wt%).

respectively (Figure 3d,e and **Table 1**). Both PHRR and THR of EP nanocomposites containing G@SiO_2, G@FeHP, G@SiO_2@FeHP or G/SiO_2/FeHP are decreased compared with those of pure EP. In detail, the PHRR and THR values of EP/0.5G@SiO_2@FeHP are decreased by 27.7% and 10.4%, and those of EP/1.0G@SiO_2@FeHP are reduced by 41.4% and 22.5% in comparison to those of pure EP. Interestingly, at the same loading of 1.0 wt%, EP/1.0G@SiO_2@FeHP presents the lowest PHRR and THR values among all EP nanocomposites, further indicating that the flame retardant

Table 1. Cone calorimeter test data of pure EP and EP nanocomposites.

Sample code	PHRR[a] [kW m^{-2}]	THR[b] [MJ m^{-2}]	PCOPR[c] [mg s^{-1}]	PCO_2PR[d] [mg s^{-1}]	TSP[e] [m^2]	TSR[f] [m^2 m^{-2}]
EP	2071 ± 41	173 ± 3.5	46.5 ± 0.9	957 ± 19	37.3 ± 0.7	4197 ± 84
EP/0.5G@SiO_2@FeHP	1500 ± 30	155 ± 3.1	36.3 ± 0.7	763 ± 15	34.2 ± 0.7	3851 ± 77
EP/1.0G@SiO_2@FeHP	1215 ± 25	134 ± 2.7	30.5 ± 0.6	606 ± 12	29.6 ± 0.6	3326 ± 66
EP/1.0G@SiO_2	1954 ± 39	165 ± 3.3	44.7 ± 0.9	866 ± 17	36.0 ± 0.7	4044 ± 81
EP/1.0G@FeHP	1376 ± 27	141 ± 2.8	33.6 ± 0.7	634 ± 13	31.4 ± 0.6	3531 ± 71
EP/1.0G/SiO_2/FeHP	1575 ± 31	152 ± 3.0	38.7 ± 0.8	763 ± 15	31.5 ± 0.6	3547 ± 71

[a] Peak heat release rate (PHRR); [b] Total heat release (THR); [c] Peak CO production rate (PCOPR); [d] Peak CO_2 production rate (PCO_2PR); [e] Total smoke production (TSP); and [f] Total smoke release (TSR).

efficiency of G@SiO_2@FeHP is higher than those of G@SiO_2, G@FeHP or G/SiO_2/FeHP.

In Figure 3f,g and Table 1, significant smoke suppression of EP/G@SiO_2@FeHP nanocomposites can be observed when analyzing the CO production rate (COPR) and TSP values. The peak CO production rate (PCOPR) and TSP values decrease gradually with the increasing G@SiO_2@FeHP content. The addition of 0.5 wt% G@SiO_2@FeHP results in 21.9% and 8.3% reductions in PCOPR and TSP relative to those of EP, respectively. When 1.0 wt% G@SiO_2@FeHP is incorporated, the PCOPR and TSP values of the nanocomposite further reduces by 34.4% and 20.6%. Notably, the PCOPR and TSP of EP/1.0G@SiO_2@FeHP exhibit much lower PCOPR and TSP than EP/1.0G@SiO_2, EP/1.0G@FeHP, and EP/1.0G/SiO_2/FeHP under the same addition of 1.0 wt%. The excellent smoke suppression of EP/1.0G@SiO_2@FeHP nanocomposite is mainly due to the synergistic effect between G, SiO_2 and FeHP, which tremendously benefits fire rescue.

The comprehensive fire-retardant performances of EP/G@SiO_2@FeHP nanocomposites were compared with those of the previously reported EP counterparts. Under the ultralow loading of 1.0 wt% G@SiO_2@FeHP, our EP/1.0G@SiO_2@FeHP features a UL-94 V-0 rating and an obvious reduction of 41.4% in PHRR relative to the untreated EP. Overall, the EP/1.0G@SiO_2@FeHP nanocomposite shows more significant PHRR decrease than previously reported EP nanocomposites that reach a UL-94 V-0 rating (Figure 3h and Table 3).[2–6,9–11,13,31,48–56] Moreover, our G@SiO_2@FeHP shows higher efficiency than previous nanofillers, such as TPP-PF_6, DIT, ZF@PZS, CQ-DOPO and ETP,[2,3,5,10,54] which usually need higher additions (2.0–3.8 wt%) to impart a UL-94 V-0 classification to EP. For other fire-retardant additives, such as FDI, DOPONH$_2$-S, N-DOPO, DCSA-Cu, PBMA-APP and TBD,[9,13,31,48,50,51] they fail to effectively suppress the heat release of the EP matrix in addition to high additions (5.0–7.3 wt%). Obviously, our G@SiO_2@FeHP outperforms previously reported fire retardants for EP due to its higher efficiency and more effective heat inhibition.

In Figure 3i and Table S3 (Supporting Information), our EP/1.0G@SiO_2@FeHP shows significant reductions in TSP and THR (20.6% and 22.5%) relative to EP. At the same loading level of 1.0 wt%, G@SiO_2@FeHP is more effective in simultaneously reducing TSP and THR compared with previous fire-retardant additives.[2,6,10,11,14,57–63] For instance, the nanofillers, e.g., f-BNNS@KH560, SPGP and LPP-$MoSe_2$,[14,58,61] can decrease the TSP of EP to some extents, but fail to effectively reduce the THR. For other fire-retardant additives, such as ZIF-67@APP, APOP, DP-MBI and EGOPC,[11,57,60,63] their addition could not lead to the prominent reductions in both THR and TSP. Thus, these results strongly demonstrate the superior flame-retardant efficiency and heat/smoke suppression of G@SiO_2@FeHP to previously reported flame-retardant additives.

2.2. Fire-Retardant Mode-of-Action

To deeply unveil the fire-retardant mode-of-action of G@SiO_2@FeHP towards EP, the residual chars of different EP samples after cone calorimetry were analyzed by digital camera, scanning electron microscopy-energy dispersive X-ray spectrometry (SEM-EDS), and Raman spectroscopy. As presented in **Figure** 4a–d and Figures S8–S10 (Supporting Information), only small amount of loose char residues are remained after the combustion of neat EP, and the char surface is covered with pores and cracks. With the incorporation of 0.5 wt% G@SiO_2@FeHP, the char layer becomes rigid and compact. Adding 1.0 wt% G@SiO_2@FeHP remarkably improves the compactness and intumescent height of char residue. Moreover, the EP/1.0G@SiO_2@FeHP char is better than the EP/1.0G@SiO_2, EP/1.0G@FeHP, and EP/1.0G/SiO_2/FeHP chars in terms of integrality and intumescent height, further confirming the condensed-phase synergistic effect of G, SiO_2 and FeHP.

The EDS results show that C, Si, P, and Fe elements are evenly distributed on the surface of EP/1.0G@SiO_2@FeHP char (Figure 4e). The P, Fe and Si-containing compounds can catalyze the formation of dense and compact char layers on the matrix surface during combustion, which effectively inhibit the exchange of flammable gasses and heat and protect the underlying matrix, thereby retarding the burning reaction.[23,58]

The degree of graphitization for chars was investigated by Raman technique. As shown in Figure 4f–h and Figure S11 (Supporting Information), the D and G band area ratio (I_D/I_G) values of char residues follow the sequence: EP/1.0G@SiO_2@FeHP (2.87) < EP/1.0G@FeHP (2.95) < EP/1.0G/SiO_2/FeHP (3.17) < EP/0.5G@SiO_2@FeHP (3.79) < EP/1.0G@SiO_2 (4.15) < EP (4.36). Clearly, the I_D/I_G value of EP char obviously decreases with the increasing G@SiO_2@FeHP content, and the I_D/I_G value of EP/1.0G@SiO_2@FeHP char is lower than those of EP/1.0G@SiO_2, EP/1.0G@FeHP, and EP/1.0G/SiO_2/FeHP chars. The lower I_D/I_G value indicates the higher graphitization degree and better high-temperature stability, which enables the char residue to achieve better protective effect.[25]

To further understand the modes of action of G@SiO_2@FeHP in EP, its flame inhibition, charring and barrier-protective layer effects are evaluated quantitatively with the aid of cone calorimetry test results (Table 1 and Tables S2 and S4, Supporting Information), as illustrated in the following equations (Equations1–3).[7]

$$\text{Flame inhibition} = 1 - \text{EHC}_{\text{EP composite}}/\text{EHC}_{\text{EP}} \quad (1)$$

$$\text{Charring effect} = 1 - \text{TML}_{\text{EP composite}}/\text{TML}_{\text{EP}} \quad (2)$$

$$\text{Barrier} - \text{protective effect} = 1 - (\text{PHRR}_{\text{EP composite}}/\text{PHRR}_{\text{EP}})/(\text{THR}_{\text{EP composite}}/\text{THR}_{\text{EP}}) \quad (3)$$

where TML represents total mass loss, and EHC refers to effective heat of combustion. It is clear that at the same 1.0 wt% loading level, as-prepared G@SiO_2@FeHP leads higher flame inhibition (14.5%), charring (13.6%) and barrier-protective layer effects (24.3%) than G@SiO_2, G@FeHP, and G/SiO_2/FeHP (see Table S4, Supporting Information). For example, the physical mixture of G, SiO_2 and FeHP, namely G/SiO_2/FeHP shows a flame

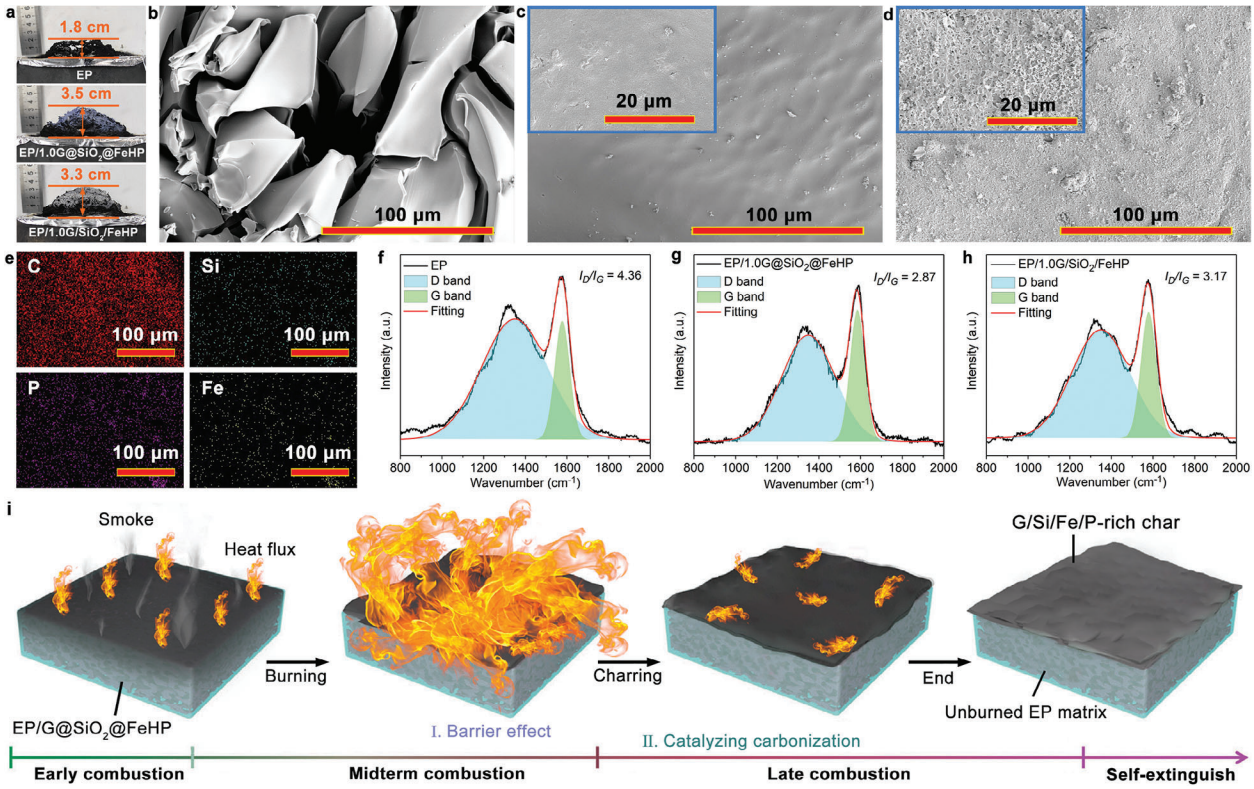

Figure 4. Flame-retardant mode-of-action. a) Digital images of char residues after cone calorimetry; SEM images of char residues for b) EP, c) EP/1.0G@SiO_2@FeHP and d) EP/1.0G/SiO_2/FeHP; e) EDS mappings of EP/1.0G@SiO_2@FeHP char; Raman spectra of f) EP, g) EP/1.0G@SiO_2@FeHP, and h) EP/1.0G/SiO_2/FeHP chars; and i) a proposed fire-retardant mode-of-action of G@SiO_2@FeHP towards EP.

inhibition effect of 8.4%, charring effect of 8.6% and barrier-protective layer effect of 13.4%. The results and comparison strongly indicate that the as-synthesized G@SiO_2@FeHP as a fire retardant for EP can function in both the gas and condensed phases, and also performs better than the simple mixture of three components (see Table 1) due to its improved dispersion and a synergy between three components.

Based on the above comprehensive analyses, it is reasonable to propose a possible fire-retardant mode-of-action of G@SiO_2@FeHP in EP (see Figure 4i). Upon exposure to the external fire, some unstable polymer chains of EP/G@SiO_2@FeHP nanocomposite begin to degrade, accompanied by the release of toxic smoke. With the increasing exposure time, the thermally stable G@SiO_2 acts as a barrier to inhibit the transfer of heat, oxygen and volatile products, thereby slowing down the burning of the matrix.[21,64] Meanwhile, the FeHP of G@SiO_2@FeHP can release phosphorous and metaphosphoric acids during combustion, which catalyze the EP matrix to dehydrate/carbonize into high-quality char layers.[57,65] Both iron compounds and G@SiO_2 enhances the compactness of char layers.[29,35] These char layers with high degree of graphitization serve as protective barriers, which obstruct the penetration of heat and oxygen and inhibit the release of combustible gases, thereby effectively suppressing the burning of the EP matrix.[54,56] In summary, the enhanced fire retardancy of EP/G@SiO_2@FeHP is mainly ascribed to the barrier and promoting carbonization effects of G@SiO_2@FeHP, as confirmed by the exceptional barrier-protective effect of EP/G@SiO_2 system.

2.3. Mechanical Properties

The mechanical properties of EP usually determine its practical applications, so it is important to assess the effects of fire retardants on the mechanical performances of EP. **Figure** 5a–e and **Table** 2 present the mechanical properties of EP and EP nanocomposites. The tensile strength, tensile modulus, and impact strength of EP are 42.9 MPa, 1.8 GPa and 7.8 kJ m^{-2}, respectively. The introduction of G@SiO_2@FeHP obviously increases the tensile strength, tensile modulus, and impact strength of EP. For example, the tensile strength, tensile modulus, and impact strength of EP/1.0G@SiO_2@FeHP nanocomposite reach 62.0 MPa, 2.9 GPa and 11.1 kJ m^{-2}, which are 44.5%, 61.1% and 42.3% higher than those of EP, respectively. At the same flame retardant content of 1.0 wt%, the tensile strength, tensile modulus, and impact strength of EP/1.0G@SiO_2@FeHP are all higher than those of EP/1.0G@SiO_2, EP/1.0G@FeHP and EP/1.0G/SiO_2/FeHP, indicative of the reinforcing and toughening effects of G@SiO_2@FeHP.

The fire-retardant and mechanical performances of EP/1.0G@SiO_2@FeHP and previous fire-retardant EP nanocomposites with a UL-94 V-0 classification were comprehensively compared in Figure 5f and **Table 3**.[3,9–11,13,31,50,53–55] Clearly, the tensile and impact strength improvements (44.5% and 42.3%) of our EP/1.0G@SiO_2@FeHP are much higher than those of previously reported fire-retardant EP systems, further demonstrating the positive effects of G@SiO_2@FeHP on the mechanical performances of EP.

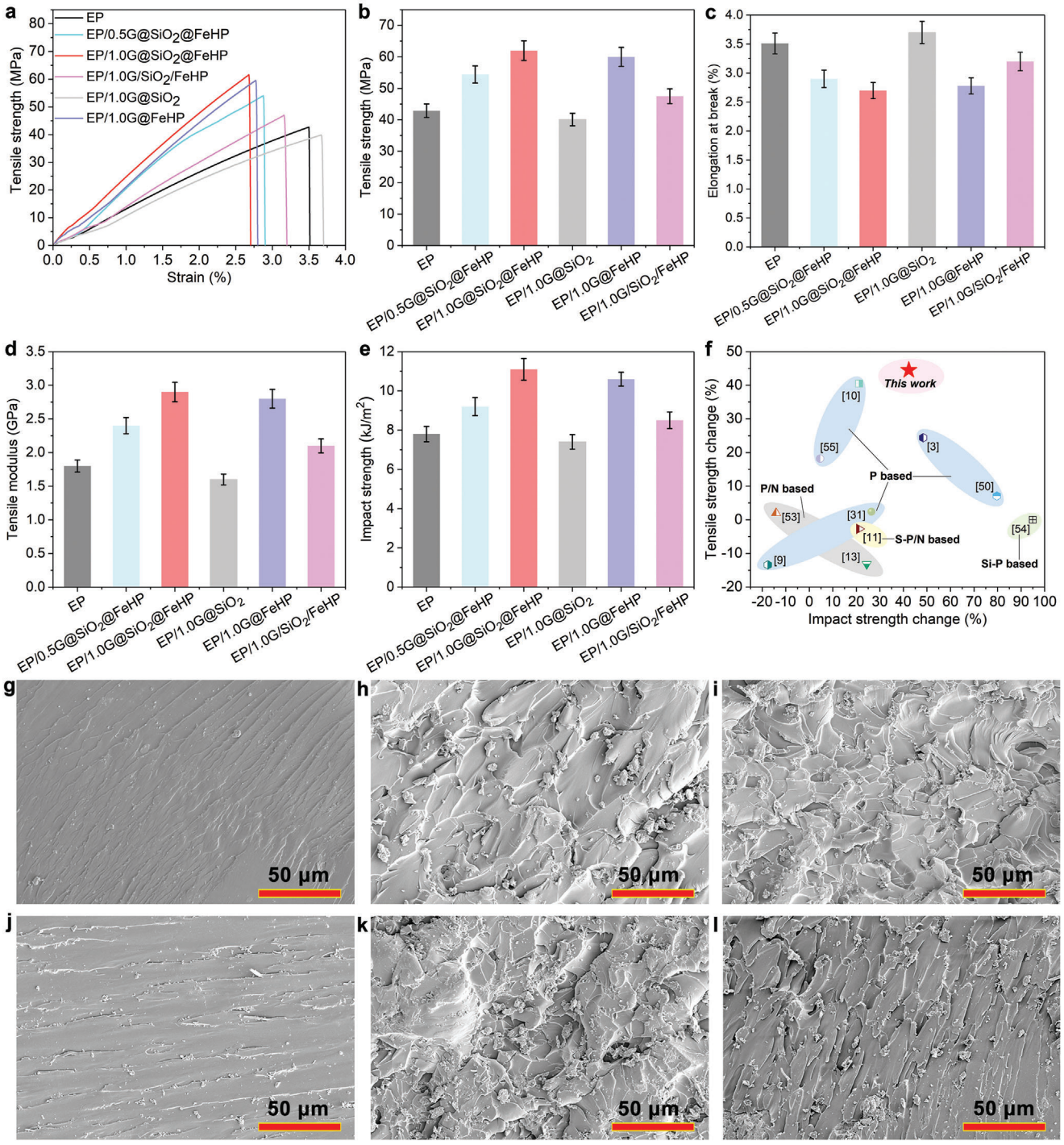

Figure 5. Mechanical performances. a) Tensile stress–stain curves, b) tensile strengths, c) elongations at break, d) tensile moduli, and e) impact strengths of EP and EP nanocomposites; f) comparison of tensile strength and impact strength variations of EP/1.0G@SiO_2@FeHP nanocomposite and previously reported EP composites with a UL-94 V-0 rating; and SEM images of fracture surfaces for g) EP, h) EP/0.5G@SiO_2@FeHP, i) EP/1.0G@SiO_2@FeHP, j) EP/1.0G@SiO_2, k) EP/1.0G@FeHP, and l) EP/1.0G/SiO_2/FeHP.

The reinforcing/toughening mechanisms of G@SiO_2@FeHP for EP were studied by analyzing the fracture surfaces of EP samples. EP exhibits smooth and regular hackle-like cross-section, indicating brittle failure (Figure 5g). The incorporation of G@SiO_2@FeHP leads to a rough and twisty fractured surface, suggesting the obvious crack propagation (Figure 5h,i). Especially for EP/1.0G@SiO_2@FeHP, the homogeneous surface morphologies with remarkably herringbone ridge-like protuberances can be observed, indicating that more fracture energy is absorbed during the crack propagation. Obviously, the

Table 2. Mechanical properties of EP and its nanocomposites.

Sample code	Tensile strength [MPa]	Elongation at break [%]	Tensile modulus [GPa]	Impact strength [kJ m^{-2}]
EP	42.9 ± 2.2	3.51 ± 0.18	1.8 ± 0.09	7.8 ± 0.39
EP/0.5G@SiO_2@FeHP	54.4 ± 2.7	2.90 ± 0.15	2.4 ± 0.12	9.2 ± 0.46
EP/1.0G@SiO_2@FeHP	62.0 ± 3.1	2.70 ± 0.14	2.9 ± 0.15	11.1 ± 0.56
EP/1.0G@SiO_2	40.1 ± 2.0	3.70 ± 0.19	1.6 ± 0.08	7.4 ± 0.37
EP/1.0G@FeHP	60.0 ± 3.0	2.78 ± 0.14	2.8 ± 0.14	10.6 ± 0.35
EP/1.0G/SiO_2/FeHP	47.5 ± 2.4	3.20 ± 0.16	2.1 ± 0.11	8.5 ± 0.43

organic phosphorus-containing segments of FeHP on the G@SiO_2 surface improves the compatibility of G@SiO_2@FeHP and EP, enabling it to form strong interfacial interaction and mechanical interlocking with the EP matrix,[25,27,28] which contribute to the energy dissipation under the external forces.[35,66,67] Moreover, the stress can effectively transfer between the EP matrix and G nanosheets when the matrix suffers from the external force. The force of SiO_2 can cause a silver pattern inside the EP matrix, which also brings about the energy dissipation.[15,68] Hence, the reinforcing/toughening effects of G@SiO_2@FeHP are mainly due to the combined action of G nanosheets, SiO_2 and FeHP.

The SEM images of fractured surfaces for EP/1.0G@SiO_2, EP/1.0G@FeHP, and EP/1.0G/SiO_2/FeHP are shown in Figure 5j–l. The cross-section of EP/1.0G@SiO_2 is very smooth (Figure 5j), which is not conducive to dissipating the energy. In addition, the obvious agglomeration of G@SiO_2 within the EP matrix can be detected, leading to the stress concentration under the external forces and thus the unsatisfied mechanical properties of EP/1.0G@SiO_2. Compared with G@FeHP, introducing G@SiO_2@FeHP results in the formation of a rougher and more irregular fracture surface with large-crinkled textures (Figure 5k), further confirming the synergistic effects of FeHP, G and SiO_2. For EP/1.0G/SiO_2/FeHP, it presents a relatively smooth cross-section (Figure 5l), indicating the poor interfacial interactions between G, SiO_2, FeHP and EP matrix, which bring about the unsatisfactory mechanical performances.[69]

The dielectric and electric performances of EP are vital for its application in the advanced electrical devices. The dielectric properties of EP and EP/1.0G@SiO_2@FeHP nanocomposite were investigated. As shown in **Figure 6**a,b, the addition of 1.0 wt% G@SiO_2@FeHP does not affect the dielectric constant and loss of EP in the frequency of 10–10^6 Hz. FeHP on the

Table 3. Comparison of fire retardant and mechanical performances of EP nanocomposites (ϕV-0[a], ΔPHRR[a], Δσm[a] and Δδm[a] refer to fire-retardant content for a UL-94 V-0 rating, PHRR reductions, tensile strength change and impact strength change, respectively; $\Delta PHRR = \frac{PHRR_{EP} - PHRR_{EP\ nanocomposite}}{PHRR_{EP}}$, $\Delta\sigma m = \frac{\sigma m_{EP\ nanocomposite} - \sigma m_{EP}}{\sigma m_{EP}}$, $\Delta\delta m = \frac{\delta m_{EP\ nanocomposite} - \delta m_{EP}}{\delta m_{EP}}$; DOPO: 9,10-dihydro-9-oxa-10-phosphaphenanthrene-10-oxide; BP: black phosphorus; APP: ammonium polyphosphate; IL: ionic liquid; P: phosphorus; N: nitrogen; Si: silicon; S: sulfur; B: boron).

Flame retardant	Type	ϕV-0[a] [wt%]	ΔPHRR[a] [%]	Δσm[a] [%]	Δδm[a] [%]	Refs.
CQ-DOPO	P based	3.5	− 22.7	+ 24.4	+ 48.4	2023[3]
FDI	P based	5.0	− 33.6	−13.4	−17.6	2023[9]
ITA	P based	2.0	− 7.2	+ 40.5	+ 21.2	2023[10]
CF-PO($OPh_)_2$	P based	6.75	− 26.2	+ 2.4	+ 26.4	2023[31]
N-DOPO	P based	7.0	− 19.6	/	/	2023[48]
BDHDP	P based	1.5	− 18.0	/	/	2022[49]
TBD	P based	7.3	− 16.3	+ 7.1	+ 79.7	2023[50]
DCSA-Cu	P based	5.0	− 29.7	/	/	2023[51]
DPOR	P based	4.8	− 27.5	+ 18.2	+ 4.6	2022[55]
TPP-PF_6	IL based	2.0	− 36.32	/	/	2023[5]
PBMA-APP	P/N based	6.0	− 2.2	−13.2	+ 24.4	2023[13]
DPPVA	P/N based	4.0	− 32.5	+ 2.0	−14.1	2023[53]
ZB-BPNs@PETA	BP based	2.0	− 41.5	/	/	2023[52]
ETP	Si-P based	2.3	0	0	+ 95	2023[54]
AgNC@BP	B-P based	5.0	− 39.0	/	/	2022[56]
ZF@PZS	Metal-P/N based	3.8	− 37	/	/	2023[2]
PHDT@FeCo-LDH	Metal-P/N based	4.0	− 28.3	/	/	2022[4]
FeHP@GO	Metal-P/N based	1.0	− 28.2	/	/	2023[6]
DP-MBI	S-P/N based	3.0	− 17.5	−2.7	+ 21.2	202 2[11]
G@SiO_2@FeHP	Fe-Si-P based	1.0	− 41.4	+ 44.5	+ 42.3	This work

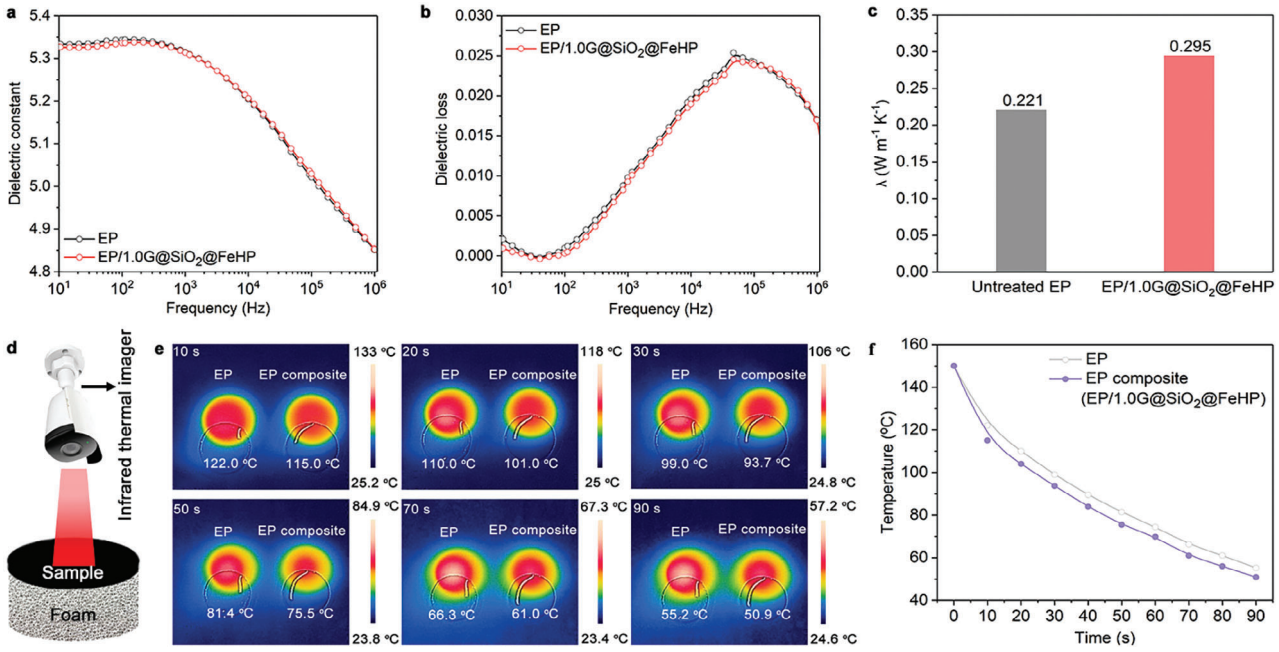

Figure 6. Dielectric and thermally conductive performances. a) Dielectric constant and b) dielectric loss curves of EP and EP/1.0G@SiO_2@FeHP nanocomposite; c) the λ values of EP and EP/1.0G@SiO_2@FeHP nanocomposite; d) the set-up of thermal diffusion test for the modules integrated with sample; and e) infrared thermal images and f) the corresponding surface temperature versus time curves of EP and EP/1.0G@SiO_2@FeHP.

G@SiO_2 surface improves the interfacial interaction between G@SiO_2@FeHP and EP, thus reducing the interfacial polarization. As a result, the dipole orientation and movement within interface are greatly restricted, thus effectively maintaining the dielectric constant and loss.[70,71] Besides, the SiO_2 nanoparticles exhibit low dielectric constant and loss, which compensate for the high dielectric constant and loss of G nanosheets.[72] Therefore, the dielectric constant and loss of EP/1.0G@SiO_2@FeHP are barely changed after the introduction of G@SiO_2@FeHP.

High electric insulating performance of EP is important for its advanced electrical application. The volume resistance of virgin EP is 2.8×10^{15} Ω cm, and that of EP/1.0G@SiO_2@FeHP nanocomposite reduces to 1.6×10^{15} Ω cm, but both are still at the same order of magnitude. It indicates the well-preserved insulating performance of EP/1.0G@SiO_2@FeHP, which is mainly due to the suppression of electron transport by SiO_2 and FeHP immobilized within the G conductive network.

The λ of both EP and EP/1.0G@SiO_2@FeHP nanocomposite was also investigated. Figure 6c shows the λ values of EP and EP/1.0G@SiO_2@FeHP nanocomposite. EP presents a λ of 0.221 W m^{-1} K^{-1}, while that of EP/1.0G@SiO_2@FeHP increases to 0.295 W m^{-1} K^{-1} by 33.5%. Due to the improved interfacial interaction of G@SiO_2@FeHP and EP, the interface phonon scattering is weakened, leading to the reduced interfacial thermal resistance and enhanced λ.[73] To explore the practical thermal diffusion of EP and EP/1.0G@SiO_2@FeHP nanocomposite, their circular specimens of the same size were placed in a 150 °C oven for 0.5 h to ensure uniform heating, and then placed on the foam at room temperature (Figure 6d). The surface temperature variation as a function of time was recorded by an infrared thermal imager, with the obtained images shown in Figure 6e,f. Obviously, the EP/1.0G@SiO_2@FeHP nanocomposite cools more quickly than virgin EP. At 90 s, the surface temperature of EP is 55.2 °C, while that of EP/1.0G@SiO_2@FeHP is 50.9 °C. The results reveal that the EP/1.0G@SiO_2@FeHP nanocomposite exhibits a better heat dissipation ability than EP due to the introduction of G@SiO_2@FeHP, which is highly in line with the λ results.

3. Conclusion

In this work, G@SiO_2@FeHP is successfully synthesized through in situ self-assembly of SiO_2 and FeHP on the G surface, and then introduced into EP to impart extraordinary fire-retardant and mechanical performances. With only 1.0 wt% G@SiO_2@FeHP, the as-fabricated EP/1.0G@SiO_2@FeHP passes a UL-94 V-0 rating and a LOI of 30.5%. In addition, the PHRR, THR, PCOPR and TSP values of EP/1.0G@SiO_2@FeHP are decreased by 41.4%, 22.5%, 34.4% and 20.6% compared with those of EP. The excellent fire retardancy of EP/G@SiO_2@FeHP is attributed to the combination of the catalytic carbonization effect of FeHP and the physical barrier effect of G@SiO_2. Moreover, 1.0 wt% G@SiO_2@FeHP increases the tensile strength, tensile modulus, and impact strength of EP/1.0G@SiO_2@FeHP to 62.0 MPa, 2.9 GPa and 11.1 kJ m^{-2}, by 44.5%, 61.1%, and 42.3%. The enhanced mechanical properties are mainly ascribed to the synergistic effects of FeHP, SiO_2 and G. The resultant EP/1.0G@SiO_2@FeHP nanocomposite also exhibits well-preserved electric insulating and dielectric properties and improved thermally conductive performances. In summary, the outstanding overall performances of EP/1.0G@SiO_2@FeHP nanocomposite allow it to find ubiquitous applications in modern industries.

4. Experimental Section

Raw Materials: The G was purchased from XF NANO (Nanjing, China). Iron nitrate nonahydrate ($Fe(NO_3)_3{\cdot}9H_2O$, 98.5%), sodium hydroxide (NaOH, 97%), 4, 4′-diaminodiphenyl methane (DDM, ≥99.0%), acetone (analytical reagent), sulfuric acid (H_2SO_4, 98%), and NaCMC (chemical pure) were obtained from Sinopharm Chemical Reagent Co., Ltd (Shanghai, China). Phenylphosphinic acid (PPIA, 98%), sodium metasilicate nonahydrate ($Na_2SiO_3{\cdot}9H_2O$, analytical reagent), and citric acid ($C_6H_8O_7$, ≥99.5%) were provided by Macklin Biochemical Co. Ltd (Shanghai, China). EP (E51, epoxide value of 0.51 mol/100 g) was purchased from China Sinopec Group.

Preparation of G@SiO_2: The G@SiO_2 was fabricated by in situ self-assembly. Briefly, 1.0 g G, 0.1 g NaCMC and 100 mL deionized water were added to agate ball mill, and ground at a speed of 1000 rpm for 12 h. After that, the G aqueous dispersion was gained, and 26.0 g $Na_2SiO_3{\cdot}9H_2O$ was added, followed by stirring at 85 °C for 0.5 h. Subsequently, 1.5 g $C_6H_8O_7$ was introduced and stirred vigorously for 0.5 h. H_2SO_4 (1 mol/L) was used to adjust the pH of mixture to 5, and then it was continuously stirred for 10 h. The target G@SiO_2 was gathered by centrifugation, washing and finally freeze-drying (pressure: 10 Pa and temperature: −80 °C) for 48 h. The weight ratio of G and SiO_2 was ca. 1:5.

Preparation of G@SiO_2@FeHP: The FeHP was loaded on the surface of G@SiO_2 by in situ self-assembly. 3.4 g G@SiO_2 and 0.1 g NaCMC was first dispersed into 200 mL deionized water by ultrasonication for 0.5 h. The mixture was transferred into a sealed agate tank, and ball milling was carried out on a planetary miller with a rotation speed of 1000 rpm for 12 h. After that, the G@SiO_2 dispersion was collected. Then, 500 mL PPIA (pH = 7.0) neutralized by NaOH (PPHA-Na: sodium phenylphosphinic acid salt) aqueous solution (0.24 mol L^{-1}) was added into the G@SiO_2 dispersion, and stirred for 0.5 h. Subsequently, the $Fe(NO_3)_3{\cdot}9H_2O$ aqueous solution (200 mL, 0.2 mol L^{-1}) was added dropwise under vigorous stirring for 8 h. Finally, the G@SiO_2@FeHP hybrid with a weight ratio of G@SiO_2 and FeHP ca. 1:5 was obtained by centrifugation from the slurry, washing with the deionized water, and freeze-drying (pressure: 10 Pa and temperature: −80 °C) for 48 h.

Fabrication of EP Nanocomposites: EP nanocomposites containing different G@SiO_2@FeHP contents were fabricated according to the following procedure. Typically, G@SiO_2@FeHP was ultrasonically dispersed in acetone for 0.5 h. Subsequently, E51 was added to the G@SiO_2@FeHP dispersion and stirred at 150 °C for 2 h. The curing agent, DDM, was then introduced and stirred at 100 °C for 5 min. After that, the mixture was defoamed under reduced pressure for 2 min. Finally, the mixture was poured into a pre-heated Teflon mold and cured at 100 °C for 2 h, and 150 °C for 3 h. The virgin EP simple without G@SiO_2@FeHP was prepared via the same process. The formulations of different EP nanocomposites are shown in Table S1 (Supporting Information).

Supporting Information

Supporting Information is available from the Wiley Online Library or from the author.

Acknowledgements

This work was financially supported by the National Natural Science Foundation of China (No. 21975185 and No. 51978239), Natural Science Foundation of Jiangsu Province (No. BK20220989), National Key R&D Program of China (No. 2022YFC3203702), and the Australian Research Council (Nos. DP190102992, FT190100188, LP220100278, DP240102628 and DP240102728).

Open access publishing facilitated by University of Southern Queensland, as part of the Wiley - University of Southern Queensland agreement via the Council of Australian University Librarians.

Conflict of Interest

The authors declare no conflict of interest.

Data Availability Statement

The data that support the findings of this study are available from the corresponding author upon reasonable request.

Keywords

epoxy resin, graphene, integrated properties, iron phenylphosphinate, silica

Received: November 21, 2023
Revised: January 27, 2024
Published online: March 1, 2024

[1] X. L. Peng, Z. K. Li, D. H. Wang, Z. F. Li, C. B. Liu, R. Wang, L. Jiang, Q. Y. Liu, P. L. Zheng, *Chem. Eng. J.* **2021**, *424*, 130404.
[2] X. M. Sun, Z. W. Li, O. Das, M. S. Hedenqvist, *Composites, Part A* **2023**, *167*, 107417.
[3] L. Zhang, Z. Li, Q. Q. Bi, L. Y. Jiang, X. D. Zhang, E. Tang, X. M. Cao, H. F. Li, J. Hobson, D. Y. Wang, *Composites, Part B* **2023**, *251*, 110490.
[4] Y. L. Sui, H. Sima, W. D. Shao, C. L. Zhang, *Composites, Part B* **2022**, *229*, 109463.
[5] M. Y. Ou, R. C. Lian, J. H. Cui, H. C. Guan, L. Liu, C. M. Jiao, X. L. Chen, *Chemosphere* **2023**, *311*, 137061.
[6] Q. Chen, L. Liu, A. L. Zhang, W. D. Wang, Z. Z. Wang, J. Z. Zhang, J. B. Feng, S. Q. Huo, X. S. Zeng, P. A. Song, *Chem. Eng. J.* **2023**, *454*, 140424.
[7] Y. X. Lu, J. B. Feng, D. Q. Yi, H. Y. Xie, Z. G. Xu, C. F. Cao, S. Q. Huo, H. Wang, P. A. Song, *Composites, Part A* **2024**, *176*, 107834.
[8] H. Y. Ma, P. A. Song, Z. P. Fang, *Sci. China. Chem.* **2011**, *54*, 302.
[9] Y. D. Wang, L. Ma, J. Yuan, Z. M. Zhu, X. M. Liu, D. S. Li, L. Q. He, F. Xiao, *Polym. Degrad. Stab.* **2023**, *212*, 110343.
[10] G. F. Ye, S. Q. Huo, C. Wang, P. A. Song, Z. P. Fang, H. Wang, Z. T. Liu, *Polym. Degrad. Stab.* **2023**, *207*, 110235.
[11] L. X. He, X. D. Liu, X. T. Zheng, Y. Q. Dong, W. B. Bai, Y. C. Lin, R. K. Jian, *Polym. Degrad. Stab.* **2022**, *203*, 110056.
[12] L. He, T. Chen, Y. Zhang, L. R. Hu, T. Wang, R. Han, J. L. He, W. Luo, Z. G. Liu, J. N. Deng, M. J. Chen, *Composites, Part B* **2022**, *230*, 109553.
[13] J. J. Yang, Y. F. Hua, J. Sun, X. M. Wang, X. Y. Gu, S. Zhang, *Adv. Energy Mater.* **2023**, *25*, 2300011.
[14] Y. L. Xiao, G. Y. Jiang, C. Ma, X. Zhou, C. Y. Wang, Z. M. Xu, X. W. Mu, L. Song, Y. Hu, *Chem. Eng. J.* **2021**, *426*, 131839.
[15] J. Yuan, Z. M. Zhu, Y. D. Wang, X. Z. Yin, X. B. Lin, *Polym. Degrad. Stab.* **2023**, *210*, 110308.
[16] Y. B. Hou, Z. M. Xu, F. K. Chu, Z. Gui, L. Song, Y. Hu, W. Z. Hu, *Composites, Part B* **2021**, *221*, 109014.
[17] H. Jiang, Y. H. Xie, R. Zhu, Y. Luo, X. X. Sheng, D. L. Xie, *Chem. Eng. J.* **2023**, *456*, 141049.
[18] A. K. Geim, *Science* **2009**, *324*, 1530.
[19] X. Wang, E. N. Kalali, J. T. Wan, D. Y. Wang, *Prog. Polym. Sci.* **2017**, *69*, 22.
[20] X. Wang, T. Chen, J. Hong, W. A. Luo, B. R. Zeng, C. H. Yuan, Y. T. Xu, G. R. Chen, L. Z. Dai, *Composites, Part B* **2020**, *200*, 108271.
[21] B. Sang, Z. W. Li, X. H. Li, L. G. Yu, Z. J. Zhang, *J. Mater. Sci.* **2016**, *51*, 8271.
[22] X. Wang, W. Y. Xing, X. M. Feng, B. Yu, L. Song, Y. Hu, *Polym. Chem.* **2014**, *5*, 1145.

[23] Q. H. Kong, Y. L. Sun, C. J. Zhang, H. M. Guan, J. H. Zhang, D. Y. Wang, F. Zhang, *Compos. Sci. Technol.* **2019**, *182*, 107748.
[24] K. P. Song, Y. T. Pan, J. Zhang, P. A. Song, J. Y. He, D. Y. Wang, R. J. Yang, *Chem. Eng. J.* **2023**, *468*, 143653.
[25] Y. Q. Shi, X. D. Xu, Z. W. Ma, B. Yu, S. Y. Fu, G. B. Huang, H. Wang, P. A. Song, *Chem. Eng. J.* **2021**, *424*, 130362.
[26] J. Zhang, Z. Li, X. L. Qi, D. Y. Wang, *Nano-Micro Lett.* **2020**, *12*, 173.
[27] J. Zhang, Z. Li, X. L. Qi, W. Zhang, D. Y. Wang, *Composites, Part B* **2020**, *188*, 107881.
[28] W. D. Wang, Z. Z. Wang, *Composites, Part A* **2021**, *149*, 106588.
[29] M. H. Zhu, L. Liu, Z. Z. Wang, *Composites, Part B* **2020**, *199*, 108283.
[30] Y. D. Wang, L. Y. Liu, L. Ma, J. Yuan, L. X. Wang, H. Wang, F. Xiao, Z. M. Zhu, *Polym. Degrad. Stab.* **2022**, *204*, 110106.
[31] G. Y. Jiang, Y. L. Xiao, Z. Y. Qian, Y. T. Yang, P. F. Jia, L. Song, Y. Hu, C. Ma, Z. Gui, *Chem. Eng. J.* **2023**, *451*, 137823.
[32] Z. Hou, H. P. Cai, C. Li, B. L. Li, H. H. Wang, *J. Appl. Polym. Sci.* **2022**, *139*, e52712.
[33] X. Q. Qiu, X. L. Wan, Z. C. Wang, Z. W. Li, J. Li, X. H. Li, Z. J. Zhang, *Composites, Part B* **2022**, *238*, 109887.
[34] S. D. Jiang, G. Tang, J. M. Chen, Z. Q. Huang, Y. Hu, *J. Hazard. Mater.* **2018**, *342*, 689.
[35] W. D. Wang, Z. Z. Wang, *Polym. Adv. Technol.* **2022**, *33*, 1496.
[36] T. Zhang, L. Lin, X. F. Zhang, H. O. Liu, X. J. Yan, J. S. Qiu, K. L. Yeung, *Mater. Lett.* **2015**, *148*, 17.
[37] L. Liu, M. H. Zhu, Z. W. Ma, X. D. Xu, S. M. Seraji, B. Yu, Z. Q. Sun, H. Wang, P. A. Song, *Chem. Eng. J.* **2022**, *430*, 132712.
[38] A. O. Oluwole, O. S. Olatunji, *Chem. Eng. J.* **2022**, *12*, 100417.
[39] Y. Ma, H. H. Di, Z. X. Yu, L. Liang, L. Lv, Y. Pan, Y. Y. Zhang, D. Yin, *Appl. Surf. Sci.* **2016**, *360*, 936.
[40] Z. Hu, G. P. Lin, L. Chen, Y. Z. Wang, *Polym. Adv. Technol.* **2011**, *22*, 1166.
[41] W. Y. Yang, J. Kim, J. Kim, *Composites, Part A* **2023**, *175*, 107797.
[42] Y. N. Wang, F. H. Wang, S. N. Dong, H. He, Y. L. Lu, J. Shi, J. J. Liu, H. Zhu, *Compos. Sci. Technol.* **2020**, *198*, 108297.
[43] Y. X. Wei, C. Deng, Z. Y. Zhao, Y. Z. Wang, *Polym. Degrad. Stab.* **2018**, *154*, 177.
[44] X. L. Pu, S. Gu, Y. F. Xiao, Y. Z. Wang, L. Chen, *Polym. Degrad. Stab.* **2022**, *206*, 110170.
[45] G. B. Lou, Z. W. Ma, J. F. Dai, Z. C. Bai, S. Y. Fu, S. Q. Huo, L. J. Qian, P. A. Song, *ACS Sustainable Chem. Eng.* **2021**, *9*, 13595.
[46] K. D. Demadis, S. D. Katarachia, M. Koutmos, *Inorg. Chem. Commun.* **2005**, *8*, 254.
[47] S. D. Jiang, Z. M. Bai, G. Tang, L. Song, A. A. Stec, T. R. Hull, Y. Hu, W. Z. Hu, *ACS Appl. Mater. Interfaces* **2014**, *6*, 14076.
[48] W. J. Zhang, M. T. Zhou, Y. C. Kan, J. Chen, Y. Hu, W. Y. Xing, *Polym. Degrad. Stab.* **2023**, *208*, 110236.
[49] S. Q. Huo, T. Sai, S. Y. Ran, Z. H. Guo, Z. P. Fang, P. A. Song, H. Wang, *Composites, Part B* **2022**, *234*, 109701.
[50] B. L. Li, L. W. Li, Y. W. Mao, H. P. Cai, *ACS Appl. Polym. Mater.* **2023**, *5*, 1756.
[51] J. W. Li, P. L. Zheng, H. Y. Liu, J. C. Sun, Y. W. Meng, H. H. Zhao, J. Wu, Y. Zheng, Q. Y. Liu, *ACS Omega* **2023**, *8*, 16080.
[52] W. J. Diao, Z. J. Liu, G. M. Yuan, E. X. Jiao, K. X. Wang, H. Yang, Z. Li, K. Wu, J. Shi, *Polym. Degrad. Stab.* **2023**, *214*, 110404.
[53] Y. F. Hua, J. X. Chen, J. Liu, J. Sun, X. Y. Gu, S. L. Jiang, S. Zhang, *Polym. Degrad. Stab.* **2023**, *209*, 110274.
[54] M. Yu, T. T. Zhang, J. Li, J. H. Tan, X. B. Zhu, *Mater. Des.* **2023**, *225*, 111529.
[55] Y. Xu, W. J. Yang, Q. K. Zhou, T. Y. Gao, G. M. Xu, Q. L. Tai, S. E. Zhu, H. D. Lu, R. K. K. Yuen, W. Yang, C. X. Wei, *Chem. Eng. J.* **2022**, *450*, 138475.
[56] L. Xia, Z. X. Miao, J. G. Dai, A. Q. Zhu, H. Xu, J. H. Zhong, Y. Chen, W. A. Luo, Y. T. Xu, C. H. Yuan, B. R. Zeng, H. S. Cao, L. Z. Dai, *Chem. Eng. J.* **2022**, *438*, 135402.
[57] W. H. Rao, J. Tao, F. H. Yang, T. Wu, C. B. Yu, H. B. Zhao, *Chemosphere* **2023**, *311*, 137047.
[58] C. B. Yu, T. Wu, F. H. Yang, W. H. Rao, H. B. Zhao, Z. M. Zhu, *Eur. Polym. J.* **2022**, *167*, 111075.
[59] Z. B. Shao, X. Song, T. C. Wang, J. Cui, W. Ye, B. Y. Xu, D. Y. Wang, *Compos. Commun.* **2022**, *36*, 101360.
[60] T. Wu, F. H. Yang, J. Tao, H. B. Zhao, C. B. Yu, W. H. Rao, *J. Colloid Interface Sci.* **2023**, *640*, 864.
[61] W. Wang, Y. Liu, Q. Wang, *Compos. Sci. Technol.* **2023**, *242*, 110161.
[62] G. F. Ye, S. Q. Huo, C. Wang, Q. Shi, L. F. Yu, Z. T. Liu, Z. P. Fang, H. Wang, *Composites, Part B* **2021**, *227*, 109395.
[63] Z. B. Shao, J. Zhang, R. K. Jian, C. C. Sun, X. L. Li, D. Y. Wang, *Composites, Part A* **2021**, *149*, 106529.
[64] C. L. Chen, G. Q. Xiao, F. Zhong, S. T. Dong, Z. W. Yang, C. Y. Chen, M. T. Wang, R. Zou, *Prog. Org. Coat.* **2022**, *163*, 106605.
[65] Q. Chen, Z. Z. Wang, *Composites, Part A* **2022**, *153*, 106738.
[66] X. Bi, H. Di, J. Liu, Y. F. Meng, Y. Y. Song, W. H. Meng, H. Q. Qu, L. D. Fang, P. A. Song, J. Z. Xu, *Adv. Compos. Hybrid Mater.* **2022**, *5*, 1743.
[67] Q. Chen, Z. W. Ma, Z. Z. Wang, L. Liu, M. H. Zhu, W. W. Lei, P. A. Song, *Adv. Funct. Mater.* **2022**, *32*, 2110782.
[68] K. Wen, Y. Q. Liu, S. L. Huang, X. G. Su, C. B. Liang, G. Z. Zhao, *Compos. Sci. Technol.* **2022**, *229*, 109666.
[69] M. H. Zhu, L. Liu, Z. Z. Wang, *J. Hazard. Mater.* **2020**, *392*, 122343.
[70] Y. X. Yuan, Y. K. Tang, Q. M. Gao, X. C. Wang, S. R. Cheng, H. F. Liu, S. S. Guan, *J. Mol. Struct.* **2022**, *1267*, 133656.
[71] N. Jia, B. Yang, X. H. Wang, N. Zhang, Y. Wang, Y. Q. Yang, R. Xia, J. S. Qian, X. X. Chen, Y. Pan, Y. C. Ke, T. Jiang, *Polym. Test.* **2023**, *117*, 107868.
[72] B. Wu, Y. Xu, N. Wu, X. Z. Tang, *Eur. Polym. J.* **2021**, *155*, 110570.
[73] Q. Chen, Z. W. Ma, M. C. Wang, Z. Z. Wang, J. B. Feng, V. Chevali, P. A. Song, *Nano Res.* **2023**, *16*, 1362.